Inorg. Chem. **2008**, *47*, 4817−4825

Modeling the Vibronic Spectra of Transition Metal Complexes: The Ligand-Field Spectrum of $[PtCl_4]^{2-}$

Adam J. Bridgeman*

School of Chemistry, Building F11, Eastern Avenue, The University of Sydney, NSW 2006, Australia

Received January 17, 2008

A framework for calculating the intensity distribution and vibrational fine structure in the polarized ligand-field spectrum of transition metal complexes using the Herzberg−Teller approach is introduced and used to model the spectrum of the $[PtCl_4]^{2-}$ ion. The model uses geometries, vibrational frequencies, and transition moments generated using density functional calculations on the ground and excited states, which arise from spin-allowed reorganization of the d electrons. The model predicts the whole spectral trace, including the polarization, the difference in the frequency of the electronic origin, the band maximum and the vertical transition energy, and the temperature dependence of the band intensities and the frequencies of the band maxima. Excitation to the $^1A_{2g}$ state is accompanied by a vibrational progression in the breathing mode of the excited state, as observed experimentally. Excitation to both the $^1B_{1g}$ and ^1E_g states is accompanied by a loss of planarity and extended vibrational progressions in two modes, and the resulting spectra are inherently of low resolution.

1. Introduction

Measurement of the electronic absorption spectrum remains the most direct method for studying the electronic energy levels and bonding in compounds. The varied colors of transition metal complexes have led to long and ongoing interest among synthetic, inorganic, and theoretical chemists as well as spectroscopists in understanding their UV/visible spectra.[1] The electronic transitions between orbitals of dominant d orbital character which give rise to these ligand-field spectra occur with energies which are readily accessible to spectrometers and to our eyes. They are traditionally interpreted using fairly simple but still relevant models, such as crystal-field and ligand-field theory.[2] The ability of such approaches to predict the number of bands and their intensities is probably the key reason for their continued incorporation into undergraduate programs and in the introductory chapters of almost all general and inorganic chemistry textbooks.

Electric dipole transitions between *d* orbitals, or between states derived wholly from a pure *d* orbital basis as assumed in ligand-field models, are forbidden by the orbital selection rule, and intensity arises through mixing with ligand and metal *p* and *f* functions. The relatively low extinction coefficients of the bands in ligand-field spectra and pale colors of many complexes, however, have been taken to be evidence of minimal *d* orbital covalency, and thus the description of ligand-field transitions as being "orbitally forbidden" has endured. Furthermore, many transition metal complexes have geometries which are centrosymmetric or are very nearly so. In such systems, Laporte's rule forbids electric dipole transitions between states of the same parity, such as those involved in ligand-field transitions. As the molecules are not stationary at the equilibrium geometry, intensity arises through mixing during certain vibrations. Such transitions are commonly *ca.* 100 times weaker than fully allowed transitions with typical extinction coefficients of 2−50 $M^{-1}cm^{-1}$. As examples of this type of complex include octahedral and square planar complexes, this is a very common case. In complexes of any but the lowest-order symmetry groups, there are always transitions whose intensity arises through vibronic coupling. Even in complexes with little or no symmetry, it is probable that vibronic coupling plays a significant role.

* E-mail: A.Bridgeman@chem.usyd.edu.au.

(1) Hitchman, M. A.; Riley, M. J. *Inorganic Electronic Structure and Spectroscopy*; Solomon, E. I., Lever, A. B. P. Ed.; Wiley: New York, 1999; Vol. 2, pp 213.

(2) Figgis, B. N.; Hitchman, M. A. *Ligand-Field Theory and its Applications*; Wiley VCH: New York, 2000.

(3) Herzberg, G.; Teller, E. *Z. Phys. Chem., Abt. B* **1933**, *21*, 410.

10.1021/ic800091y CCC: $40.75
Published on Web 05/07/2008

The first analysis of vibronic transitions was carried out by Herzberg and Teller,[3] within the Born−Oppenheimer approximation, by expressing the electronic wave function for any nuclear configuration as an expansion in the "clamped nuclei" wave functions. Symmetry dictates that only motion along certain vibrations, called inducing modes, can produce the necessary parity mixing to produce intensity. Recently, a number of groups have developed Herzberg−Teller (HT) methods for calculating the vibrational structure of Laporte forbidden transitions in organic molecules.[4–7]

Modern electronic structure methods have made realistic and reliable calculations of excited states possible. The goal of the work described in this paper is to provide a framework for calculating the intensity of ligand-field spectra in centrosymmetric complexes and the fairly complicated vibrational fine structure often observed in ligand-field bands. Through knowledge of the ground- and excited-state potential energy surfaces and the dependence of the electronic transition moment along vibrational coordinates, this method produces *ab initio* simulated spectra of parity-forbidden but vibronically allowed electronic transitions for transition metal complexes.

The $[PtCl_4]^{2-}$ ion is probably the archetypical square-planar complex, and as a result of its simple and highly symmetric geometry, its structure was confirmed by one of the very first crystallographic studies of a coordination compound.[8] A number of studies have been reported on the transition energies[9–11] and the vibronic coupling[12–18] in this system. As polarized crystal spectra have previously been reported on this system at different temperatures, it is an obvious test case for developing a framework for the calculation of the vibronic spectra of transition metal complexes.

Grimme has recently published an excellent review of the calculations of electronic spectra.[19] Time-dependent density functional theory (TDDFT) is often the method of choice for modeling the electronic spectra of transition metal complexes, where a number of closely separated states is often observed. In large complexes, TDDFT is usually the only high-level technique that can presently be applied. As it has already[11] been used successfully for modeling the ligand-field transition energies for the $[PtCl_4]^{2-}$ ion, it is used in all of the calculations reported here.

2. Theory

In the Born−Oppenheimer approximation, the molecular wave function can be written as a product of an electronic function Φ and a vibrational wave function χ, which are dependent on the electronic coordinates q and the nuclear coordinates Q. The crude adiabatic or "clamped nuclei" approximation gives these electronic wave functions at some chosen molecular configuration, usually the ground-state equilibrium geometry, Q_0. In a centrosymmetric system like $[PtCl_4]^{2-}$, the ligand-field states in this approximation have *gerade* (g) symmetry, and a transition between two such states, $\Phi_{g1} \rightarrow \Phi_{g2}$, is parity-forbidden. Distortion along *ungerade* (u) vibrations can lower the symmetry to a point group in which mixing[1] of the g and u states becomes possible:

$$\Phi_1 = \Phi_{g1} + \sum_i \sum_j c_{1ij}\Phi_{ui},\ \Phi_2 = \Phi_{g2} + \sum_i \sum_j c_{2ij}\Phi_{ui} \quad (1)$$

where the summations are over all of the u states and normal modes, labeled i and j, respectively. To first-order, the coefficients are obtained using the perturbation $\Delta V(q,Q)$, the dependence of the electronic coordinates q on the normal mode Q:

$$c_{1ij} = Q_{uj}\frac{\langle \Phi_{g1}|\Delta V(q,Q_0)|\Phi_{ui}\rangle}{E_{ui}-E_{g1}}, c_{2ij} = Q_{uj}\frac{\langle \Phi_{g2}|\Delta V(q,Q_0)|\Phi_{ui}\rangle}{E_{ui}-E_{g2}} \quad (2)$$

Substitution of these HT wave functions into the transition moment integral then gives nonzero terms in **r** polarization for normal modes with representations:

$$\Gamma(Q_{uj}) = \Gamma(\Phi_{g1}) \times \Gamma(\Phi_{g2}) \times \Gamma(\mathbf{r}) \quad (3)$$

As well as leading to the vibronic selection rules, this analysis shows that the largest amount of mixing and hence the strongest transitions will occur when there are nearby u states ("intensity borrowing") and that a good description of the electronic spectrum is necessary to treat the problem well. This approach neatly shows the physical source of vibronically sourced intensity and was used previously, in a semiempirical treatment within the ligand-field formalism, in our previous work on $[PtCl_4]^{2-}$ and other centrosymmetric and near centrosymmetric transition metal complexes.[12–14]

As many electronic structure programs now routinely allow direct calculation of transition moments, a more practical framework is developed by expanding the transition moment M as a Taylor series in the normal coordinates:

$$M = M(0) + \sum_j \left(\frac{\partial \mathrm{M}}{\partial Q_j}\right)_0 Q_j + \frac{1}{2}\sum_{j,k}\left(\frac{\partial^2 M}{\partial Q_j\,\partial Q_k}\right)_0 Q_j Q_k + \ldots \quad (4)$$

The first term represents the transition moment in the clamped nuclei wave functions of the equilibrium geometry. As outlined above, this term is zero for ligand-field transitions in centrosymmetric complexes, such as in the $[PtCl_4]^{2-}$ ion studied here. For other geometry types, this term may not be zero, and the series is often truncated after this term, leading to the Franck−Condon (FC) approximation. However, even in such systems, the first term may not be dominant, and it is still necessary to work beyond the FC approximation.[20]

Truncation of the series after the second term gives the FC−HT approximation. If $M(0)$ is zero and the series is truncated after the second term, the approach is called the HT approximation. As the molecular wave function, Ψ, is a product of the electronic wave function, $\Phi(q,Q)$ and the vibrational wave function, $\chi(Q)$, the transition moment for absorption at the HT level is

(4) Berger, R.; Fischer, C.; Klessinger, M. *J. Phys. Chem. A* **1998**, *102*, 7157.
(5) Dierksen, M.; Grimme, S. *J. Chem. Phys.* **2004**, *120*, 3544.
(6) Johnson, P. M.; Xu, H.; Sears, T. J. *J. Chem. Phys.* **2006**, *125*, 164330.
(7) Kokkin, D. L.; Reilly, N. J.; Troy, T. P.; Nauta, K.; Schmidt, T. W. *J. Chem. Phys.* **2007**, *126*, 84304.
(8) Dickinson, R. G. *J. Am. Chem. Soc.* **1922**, *44*, 2404.
(9) Gray, H. B.; Ballhausen, C. J. *J. Am. Chem. Soc.* **1963**, *85*, 260.
(10) Vanquickenborne, L. G.; Ceulemans, A. *Inorg. Chem.* **1981**, *20*, 796.
(11) Wang, F.; Ziegler, T. *J. Chem. Phys.* **2005**, *123*, 194102.
(12) Bridgeman, A. J.; Gerloch, M. *Mol. Phys.* **1993**, *79*, 1195.
(13) Bridgeman, A. J.; Gerloch, M. *Inorg. Chem.* **1995**, *34*, 4370.
(14) Bridgeman, A. J.; Gerloch, M. *Coord. Chem. Rev.* **1997**, *165*, 315.
(15) Lanthier, E.; Reber, C., Jr *Chem. Phys.* **2006**, *329*, 90.
(16) Kovarskaya, B. P.; Kovarskii, V. A. *Theor. Exp. Chem.* **1971**, *4*, 511.
(17) Preston, D. M.; Güntner, W.; Lechner, A.; Gliemann, G.; Zink, J. I. *J. Am. Chem. Soc.* **1988**, *110*, 5628.
(18) Reber, C.; Zink, J. I. *J. Phys. Chem.* **1991**, *95*, 9151.
(19) Grimme, S. *Rev. Comput. Chem.* **2004**, *20*, 153.
(20) Bridgeman, A. J.; Jupp, K. M.; Gerloch, M. *Inorg. Chem.* **1994**, *33*, 5424.

$$M = \sum_{j}^{3n-6} \left(\frac{\partial M_{12}}{\partial Q_j}\right)_0 \int \chi_{1j} Q_j \chi_{2j}\, \mathrm{d}Q_j = \sum_{j}^{3n-6} \left(\frac{\delta M_{12}}{\delta Q_j}\right)_0 \langle 1|Q_j|2\rangle \quad (5)$$

The first term represents the dependence of the transition moment for the electronic transition. Comparison of eqs 5 and 1 shows that

$$\left(\frac{\partial M_{12}}{\partial Q_j}\right)_0 = \sum_i \left(\frac{\partial c_{1ij}}{\partial Q_j}\right)_0 \langle \Phi_{g1}|er|\Phi_{ui}\rangle + \sum_i \left(\frac{\partial c_{2ij}}{\partial Q_j}\right)_0 \langle \Phi_{g2}|er|\Phi_{ui}\rangle \quad (6)$$

This form again emphasizes that the induced intensity is borrowed from nearby parity-allowed transitions.

For each inducing mode, the transition moment is calculated along the normal mode and the first derivative obtained numerically. For well-behaved cases, where higher-order terms in eq 4 are of low importance, the moment will be almost linear, will be symmetric about the origin, and, for HT systems, will pass through zero at the origin. In such cases, only a single transition moment calculation needs to be performed along the normal coordinate of each potential inducing mode, defined by eq 3.

The vibrational wave functions for the ground and excited states can be written as products of the same harmonic modes, $|j^a k^b l^c ...>$ and $|j^x k^y l^z ...>$, respectively, where the superscripts label the number of quanta in each mode. Using recursion relationships,[21] the $<1|Q_j|2>$ integrals in eq 5 become

$$\langle j^a k^b l^c ...|Q_j|j^x k^y l^z ...\rangle = \alpha_j^{1/2}\left[\left(\frac{x+1}{2}\right)^{1/2}\langle j^a|j^{x+1}\rangle + \left(\frac{x}{2}\right)^{1/2}\langle j^a|j^{x-1}\rangle\right]\langle k^b l^c ...|\, k^y l^z ...\rangle \quad (7)$$

where $\alpha_j = h/(4\pi^2 c\bar{\nu}_j)$. The terms in the square bracket involving the inducing mode are only nonzero if $\Delta\nu_j = \pm 1$. The $\langle k^b l^c ...|k^y l^z ...\rangle$ term represents the FC integrals for the remaining modes.

If the ground electronic state is not vibrationally excited, the electronic transition must be accompanied by the simultaneous excitation of one quanta of the inducing mode, $\Delta\nu_j = +1$. The lowest-energy line in the electronic spectrum will have a "false origin" corresponding to the energy of the pure electronic transition plus one quantum in the inducing mode, $\Delta E^{0-0} + \bar{\nu}_j$. The FC integrals for the remaining modes will then give progressions in other modes built upon this origin. Typically, these FC integrals are small except for totally symmetric modes and for modes which send the ground-state molecule toward the geometry of the excited state.

If the inducing mode has one or more quanta in the ground state, then transitions with $\Delta\nu_j = \pm 1$ are possible and progressions will be produced for both $\Delta E^{0-0} \pm \bar{\nu}_j$, giving a false origin at lower energy than the pure electronic transition.

The two terms in the square bracket represent the classical vibrational amplitude of the inducing mode and increase as the number of quanta in the inducing mode grows. This, together with the presence of progressions from two false origins, leads to the transition moment increasing with temperature.

In transition metal complexes, ligand-field transitions are usually associated with excitations of electrons into highly *d* antibonding orbitals, leading to bond lengthening and even changes in molecular shape. The normal modes of the ground and excited states are not the same. It is necessary to describe the excited-state modes in terms of the ground state (or vice versa) in order to calculate the required vibrational overlap integrals in eq 6. This is conveniently achieved using the Duschinsky transformation,[22] requiring knowledge of the ground- and excited-state geometries, vibrational frequencies, and normal modes.

Transition energies obtained from TDDFT calculations correspond to the vertical transition from the bottom of the potential curve of the ground state. From this, the energy of the pure electronic transition, ΔE^{0-0}, must be calculated using the energy difference between the excited state in its equilibrium geometry and in the ground-state geometry and using the zero-point energies of the two states.

The electronic spectrum of the $[PtCl_4]^{2-}$ ion, like that of most transition metal complexes, consists of a number of overlapping ligand-field bands together with the tail of an intense high-energy band originating from charge-transfer transitions. Ligand-field bands are often broad, and resolution of individual vibronic lines is rare. When vibrational progressions are observed, they are commonly seen as a partially resolved structure on the envelope of the electronic band.

3. Computational Details

Calculations have been performed using the ADF program,[23,24] at the BP86[25] level with triple-ζ (TZ2P) Slater-type orbital basis sets and relativistic effects at the ZORA level,[26] and using the Gaussian 03 program,[27] at the B3LYP[28] level with LANL2DZ double-ζ Gaussian-type valence orbital basis sets and quasi-relativistic effective core potentials. In addition to calculations on the pseudogas phase $[PtCl_4]^{2-}$ ion, environmental effects have been included using the COSMO model[29] in ADF and the PCM model[30] in Gaussian 03 and a variety of dielectric constants.

TDDFT has been used to obtain vertical transition energies. First derivatives of the transition moment along inducing modes have been obtained numerically through calculations at displacements along the mass-weighted normal modes. In ADF, TDDFT calculations have been performed using the SAOP potential,[31] which has the correct asymptotic behavior. In all calculations below, spin−orbit coupling has not been included, and only the singlet−singlet transitions have been modeled.

For each transition, polarization, and inducing mode, the intensity for the vibronic transitions has been calculated using the HT transition moment given in eq 5 and the FC factor given by eq 7. For each inducing mode, this involves several steps. The value of $[(\delta M)/(\delta Q)]_0$ was obtained by performing 50 separate TDDFT calculations of the transition moment along the mode and numerically measuring its slope. The FC factors were calculated using

(21) Califano, S. *Vibrational States*; Wiley: New York, 1979.
(22) Duschinsky, F. *Acta Physicochim. URSS* **1937**, *7*, 551.
(23) (a) te Velde, G.; Bickelhaupt, F. M.; Baerends, E. J.; Fonseca Guerra, G.; Snijders, J. G.; Ziegler, T. *J. Comput. Chem.* **2001**, *22*, 931. (b) Fonseca Guerra, C.; Snijders, J. G.; te Velde, G.; Baerends, E. J. *Theor. Chem. Acc.* **1998**, *99*, 391.
(24) *ADF2002.02*; SCM, Theoretical Chemistry, Vrije Universiteit: Amsterdam, The Netherlands. http://www.scm.com (accessed Apr 2008).
(25) (a) Becke, A. D. *Phys. Rev. A: At., Mol., Opt. Phys.* **1988**, *38*, 3098. (b) Perdew, J. P. *Phys. Rev. B: Condens. Matter Mater. Phys.* **1986**, *33*, 8822. (c) Perdew, J. P. *Phys. Rev. B: Condens. Matter Mater. Phys.* **1986**, *34*, 7406.
(26) van Lenthe, E.; Ehlers, A. E.; Baerends, E. J. *J. Chem. Phys.* **1999**, *110*, 8943.
(27) Frisch, M. J. et al. *Gaussian 03*, revision C.02; Gaussian, Inc.: Wallingford, CT, 2004.
(28) Stephens, P. J.; Devlin, F. J.; Chabalowski, C. F.; Frisch, M. J. *J. Phys. Chem.* **1994**, *98*, 11623.
(29) (a) Klamt, A.; Schûûrmann, G. *J. Chem. Soc., Perkin Trans.* **1993**, *2*, 799. (b) Andzelm, J.; Kõlel, C.; Klamt, A. *J. Chem. Phys.* **1995**, *103*, 9312. (c) Klamt, A. *J. Chem. Phys.* **1995**, *99*, 2224. (d) Model implemented in ADF by Pye, C. C.; Ziegler, T. *Theor. Chem. Acc.* **1999**, *101*, 396.
(30) Cossi, M.; Barone, V. *J. Chem. Phys.* **2001**, *115*, 4708.
(31) Schipper, P. R. T.; Gritsenko, G. V.; van Gisbergen, S. J. A.; Baerends, E. J. *J. Chem. Phys.* **2000**, *112*, 1344.

Table 1. Calculated Pt−Cl Bond Length (pm) and Vibrational Frequencies (cm^{-1}) for the Ground State of $[PtCl_4]^{2-}$ Using the BP86 Functional and TZ2P Basis Set with (a) No Solvent and (b) Water and Using the B3LYP Functional and LanL2DZ Basis Set with (c) No Solvent and (d) Water

	a	b	c	d	experiment
bond length	2.37	2.34	2.47	2.45	2.32[34]
			Vibrational Frequencies		
ν_1 (a_{1g})	288	309	267	274	329[35]
ν_2 (a_{2u})	129	126	120	109	173
ν_3 (b_{1g})	265	289	254	268	302
ν_4 (b_{2g})	142	145	133	134	194
ν_5 (b_{2u})	78	85	73	84	
ν_6 (e_u)	145	150	134	136	195
ν_7 (e_u)	272	292	280	282	325

the optimized ground and excited-state geometries and frequencies with the program MOLFC, developed by Borrelli and Peluso.[32] These values were then combined, *via* eq 5, to give the transition moment for the vibronic line. The energy of each vibronic transition is given by the difference between the energies of the states involved (including the pure electronic energy and the difference in the vibrational energy due to changes in the number of quanta in each vibrational mode).

When the calculated values for the transition energy and intensity of each vibronic line were used, the overall spectral traces were generated and combined using the program spectralPlot,[33] assuming Lorentzian band shapes. At this stage, the line widths of the individual vibronic lines, which depend on factors beyond the scope of the present model such as rotational energy and environmental effects, were set at arbitrary but consistent values to yield spectra with "high" and "low" resolution. These lines naturally broaden with temperature, leading to decreased resolution, as illustrated in the Supporting Information. The effect of temperature has been modeled using the simulated spectra for $v = 0$ and $v = 1$ levels of each inducing mode and Boltzmann populations.

4. Results

Ground State. The ground state of $[PtCl_4]^{2-}$ has a square-planar geometry with D_{4h} symmetry and, with the C_2' axes running along the Pt−Cl bonds, the configuration $(a_{1g})^2(b_{2g})^2(e_g)^4(b_{1g})^0$. These orbitals are primarily platinum *d* orbital in character and correspond to d_{z^2} (a_{1g}), d_{xy} (b_{2g}), $d_{xz,yz}$ (e_g), and $d_{x^2-y^2}$ (b_{1g}). The ligand-field transitions arise from transitions into the strongly antibonding $d_{x^2-y^2}$ function.

Table 1 lists the geometrical parameters and vibrational frequencies for the $^1A_{1g}$ ground state. As can be seen from the comparison with experimental data, treatment of the complex as a pseudo gas-phase species is a poor model for its behavior in the solid state or solution. The inclusion of additional basis functions, including polarization functions, does not greatly improve the results.

The inclusion of solvent increases the accuracy of the calculations, suggesting that the main source of error is the lack of environmental stabilization of the anion in the gas phase. The introduction of solvent in both the COSMO and PCM models causes a shortening of the bonds and an increase in all of the vibrational frequencies except for the a_{2u} mode, but the effect of the actual polarity of the solvent is quite small. The decrease in the calculated frequency of the a_{2u} mode in solvent is probably due to the polarity of the complex that is induced by motion along this coordinate. A scaling of *ca.* 0.86 is required for the LanL2DZ results, and this is adopted for the excited states and in the calculation of the FC factors and simulations described below.

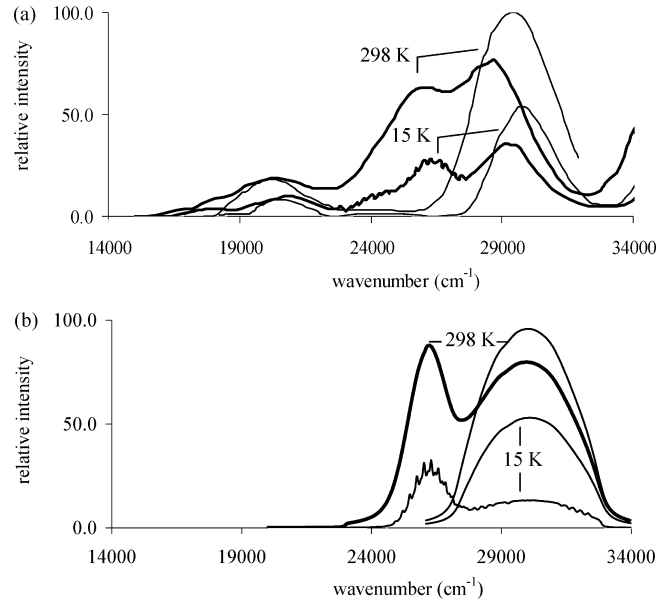

Figure 1. Electronic spectrum of K_2PtCl_4 showing (a) an experimental spectrum adapted from ref 39 and (b) simulated spectrum for spin-allowed transitions, with *z* polarized lines (light lines) and *x*,*y* polarized light (dark lines) at 15 and 298 K. The simulated spectra have been shifted from the calculated frequencies to match the experimental energies and to provide resolution of the two bands.

From the $^1A_{1g}$ ground state, three spin-allowed ligand-field transitions are possible, corresponding to the excitation of an electron into the lowest unoccupied molecular orbital (b_{1g}) from a_{1g} ($^1B_{1g} \leftarrow {}^1A_{1g}$), e_g ($^1E_g \leftarrow {}^1A_{1g}$), and b_{2g} ($^1A_{2g} \leftarrow {}^1A_{1g}$). The $^1B_{1g} \leftarrow {}^1A_{1g}$ excitation can be induced in *x*,*y* polarization by e_u modes (ν_6 and ν_7) and in *z* polarization by b_{2u} modes (ν_5). The $^1E_g \leftarrow {}^1A_{1g}$ excitation can be induced in *x*,*y* polarization by both a_{2u} (ν_2) and b_{2u} modes (ν_5) and in *z* polarization by e_u modes (ν_6 and ν_7). The $^1A_{2g} \leftarrow {}^1A_{1g}$ excitation can be vibronically induced only in *x*,*y* polarization by e_u modes (ν_6 and ν_7). The two e_u modes are in-plane motions with dominant bending (ν_6) and stretching (ν_7) character. The b_{2u} (ν_5) and a_{2u} (ν_2) modes are out-of-plane motions which send the complex toward a tetrahedral and a square-pyramidal geometry, respectively. The polarized spectrum of K_2PtCl_4 at 15 and 298 K is shown in Figure 1.

$^1A_{2g}$ State. Excitation of an electron from the weakly π-antibonding d_{xy} orbital into the strongly σ-antibonding $d_{x^2-y^2}$ orbital causes a lengthening of the bonds by *ca.* 12 pm, but the D_{4h} symmetry is maintained. Table 2 lists the vertical excitation energy and scaled vibrational frequencies for the $^1A_{2g}$ state. The a_{1g} frequency is decreased by *ca.* 80%. This excitation is induced by either of the e_u modes and is vibronically allowed only in *x*,*y* polarization. In our previous studies,[12,13] only the bending e_u mode was considered due

(32) Borrelli, R.; Peluso, A. *J. Chem. Phys.* **2003**, *119*, 8437.
(33) Bridgeman, A. J. *spectralPlot*; The University of Sydney: Sydney, 2007.
(34) Mais, R. H.; Owston, P. G.; Wood, A. M. *Acta Crystallogr., Sect. B* **1972**, *28*, 393.
(35) (a) Hendra, P. J. *J. Chem. Soc. A* **1967**, 1298. (b) Fertel, J. H.; Perry, C. *J. Phys. Chem. Solids* **1965**, *26*, 1773.

Table 2. Vertical Excitation Energies (cm^{-1}) Using SAOP and B3LYP and Scaled Vibrational Frequencies (cm^{-1}) for the Excited States of $[PtCl_4]^{2-}$ Using the B3LYP Functional and LanL2DZ Basis Set with Water Solvent

	$^1A_{1g}$	$^1A_{2g}$	^1E_g ($^1B_1$)	$^1B_{1g}$ ($^1B_2$)
Vertical (and Pure Electronic) Excitation Energies				
SAOP		23800 (22000)	23500 (20700)	27500 (23600)
B3LYP		22900 (21800)	24500 (23000)	22100 (20500)
experiment		26050	29575	36500
Vibrational Frequencies				
ν_1 (a_{1g})	329	275	272 (a_1)	261 (a_1)
ν_2 (a_{2u})	127	124	74 (a_1)	92 (b_2)
ν_3 (b_{1g})	313	138	216 (a_1)	188 (b_2)
ν_6 (b_{2g})	156	146	50 (a_2)	109 (b_1)
ν_5 (b_{2u})	98	41	47 (a_1)	58 (a_1)
ν_6 (e_u)	157	116	79 (b_1), 102 (b_2)	99 (e)
ν_7 (e_u)	319	263	247 (b_1), 247 (b_2)	250 (e)

to its higher vibrational amplitude and the practical limitations of the semiempirical approach used. Figure 2 shows the calculated transition moment as a function of displacement along both e_u modes. Although there is some curvature at larger displacements, the moment varies approximately linearly and is symmetric about the origin so that the $[(\partial^2 M)/(\partial Q_j \partial Q_k)]_0$ terms in eq 4 are probably of low importance.

Analysis of the Duschinsky transformation from the ground- to the excited-state normal modes shows that only the e_u modes become mixed by the change in geometry and that even this is minimal. FC integrals suggest that progressions in the totally symmetric stretching (ν_1) will be observed with the band maximum corresponding to the transition to $\nu' = 6$. The observation of this progression is consistent with the increase in bond length in the excited state.

Figures 3 and 4 show the simulated spectrum induced by the ν_6 and ν_7 modes, respectively, and Figure 5 shows their sum. The low-temperature spectrum is dominated by transitions from the ground vibrational level. For both e_u modes, the contributions consist of a progression in ν_1 of about 10 lines built upon the false origins of $\Delta E^{0-0} + \bar{\nu}_6$ and $\Delta E^{0-0} + \bar{\nu}_7$ shown in Figures 3a and 4a, respectively.

The first visible member of each progression is actually to the $\nu' = 1$ level of ν_1 so that there is a fairly large gap between the pure electronic transition and the first line in the spectrum. The combined spectrum, shown in Figure 5a, thus consists of two overlapping progressions which are separated by the difference in the frequency of the inducing modes: $\bar{\nu}_7 - \bar{\nu}_6 \sim 140$ cm^{-1}, from Table 1. The two

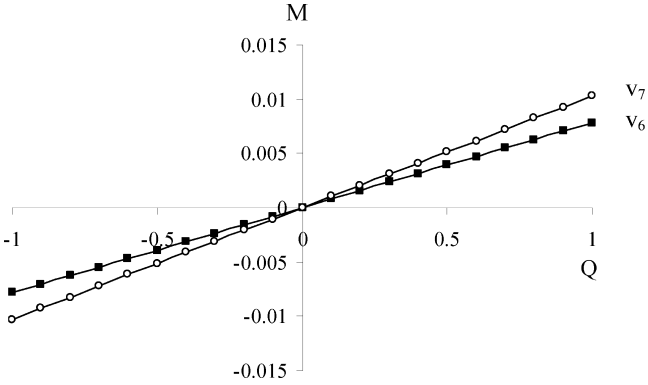

Figure 2. $^1A_{2g} \leftarrow {}^1A_{1g}$ transition moment as a function of displacement along the e_u modes for $[PtCl_4]^{2-}$ calculated using SAOP.

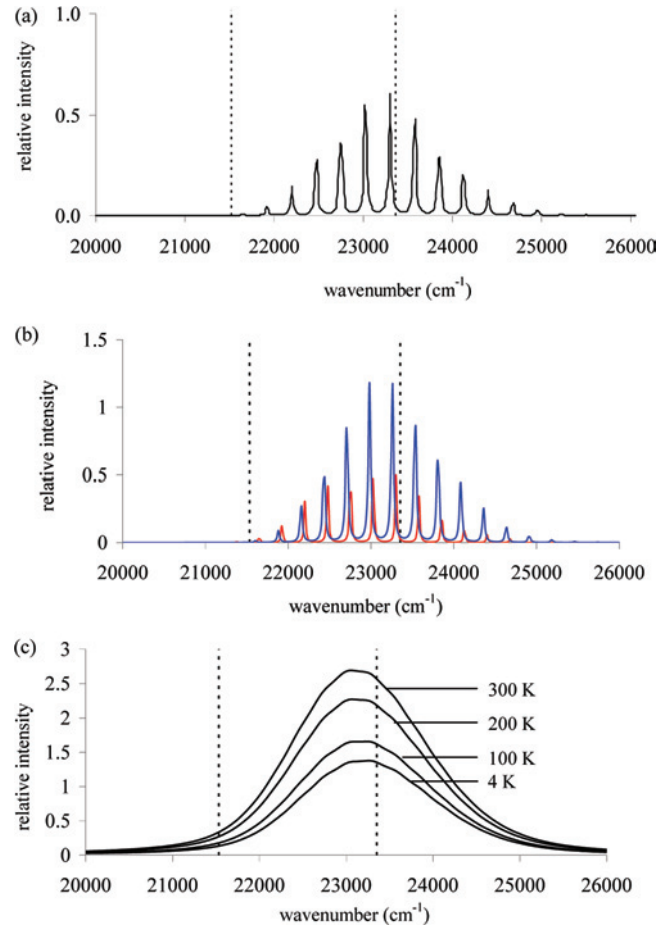

Figure 3. Simulated spectrum for $^1A_{2g} \leftarrow {}^1A_{1g}$ induced by ν_6 showing (a) the spectrum from $\nu'' = 0$, (b) the spectra from $\nu'' = 1$ to $\nu' = 0$ (red) and to $\nu' = 2$ (blue), and (c) a low-resolution spectrum as a function of the temperature. The dotted vertical lines show the pure electronic transition and the vertical transition.

progressions differ in intensity due to both the $[(\partial M_{12})/(Q_j)]_0$ term in eq 5 and the vibrational amplitude term in eq 7. As shown in Figure 2, $[(\partial M_{12})/(\partial Q_7)]_0 > [(\partial M_{12})/(\partial Q_6)]_0$, so unit displacement along the stretching mode generates more parity mixing than displacement along the bending mode. However, the vibrational amplitude term, with its $1/\bar{\nu}_j$ dependence, is larger for the latter and, as shown in Figure 5a, the total intensity generated by $\nu_6 > \nu_7$ with a ratio of *ca.* 3:2.

Experimentally, this transition has been assigned[36] from its polarization to a band with a maximum at *ca.* 26 050 cm^{-1}. In their recent TDDFT study, Wang and Ziegler[11] assigned this band to a transition to a $^3B_{1g}$ state on the basis of its calculated energy. The original assignment, however, seems more likely given the relatively high intensity of the band. As shown in Table 2, the transition energy calculated using the SAOP functional is closer to the experimental value than that obtained using the B3LYP functional but still underestimates it by over 2000 cm^{-1}. The inclusion of spin−orbit coupling reduces[11] this error by *ca.* 1000 cm^{-1}. The anionic charge of the complex is also likely to affect the accuracy of the present approach.

(36) Patterson, H. H.; Godfrey, J. J.; Khan, S. M. *Inorg. Chem.* **1972**, *11*, 2872.

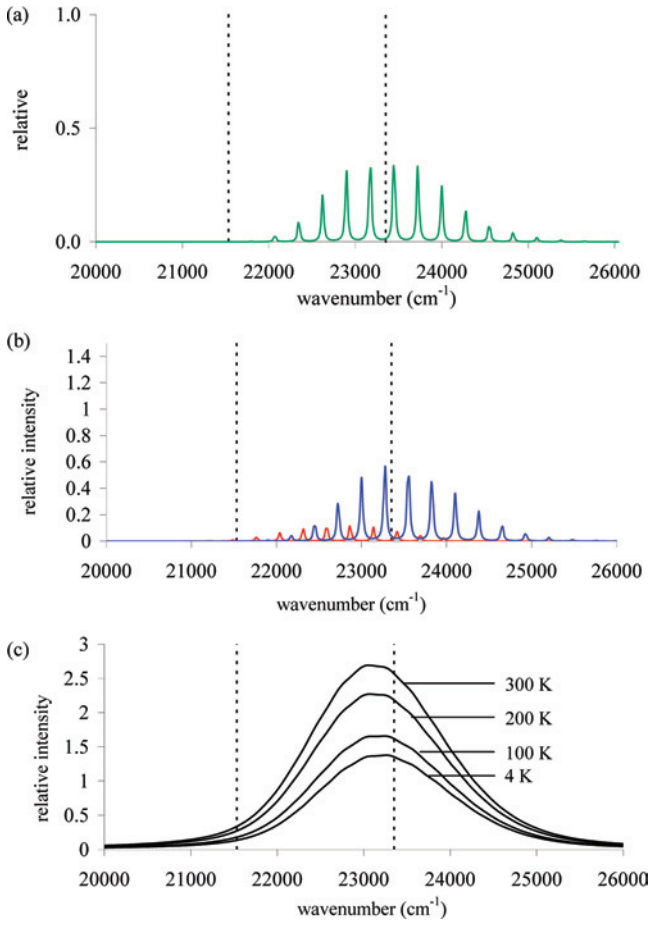

Figure 4. Simulated spectrum for $^1A_{2g} \leftarrow {}^1A_{1g}$ induced by ν_7 showing (a) the spectrum from $\nu'' = 0$, (b) the spectra from $\nu'' = 1$ to $\nu' = 0$ (red) and to $\nu' = 2$ (blue), and (c) a low-resolution spectrum as a function of the temperature. The dotted vertical lines show the pure electronic transition and the vertical transition.

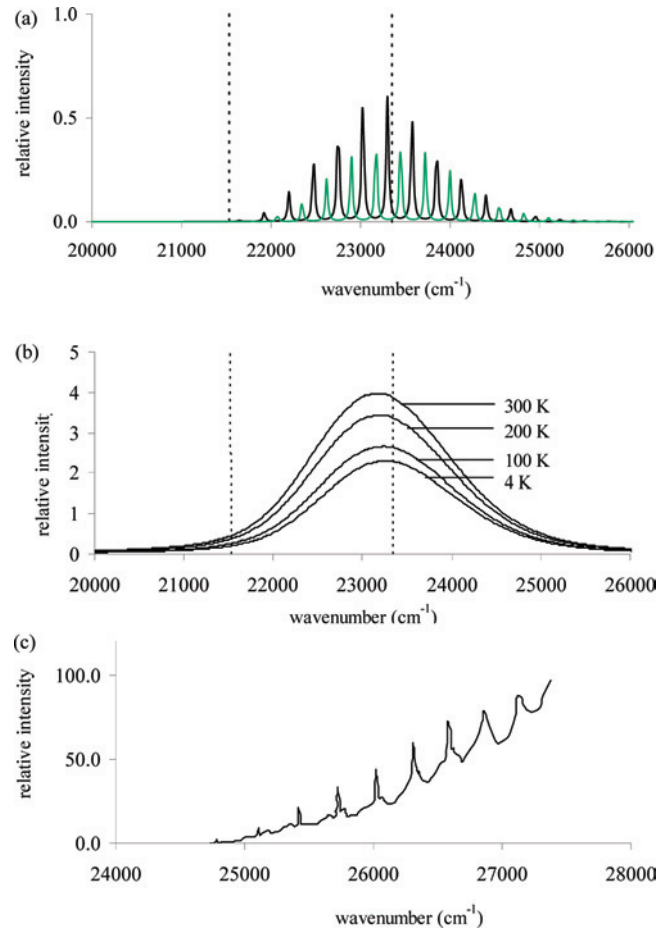

Figure 5. Spectrum for the $^1A_{2g} \leftarrow {}^1A_{1g}$ transition showing (a) the combined ν_6 and ν_7 simulated spectrum from $\nu'' = 0$, (b) the overall low-resolution simulated spectrum as a function of the temperature, and (c) the experimental spectrum, adapted from ref 36 for a $K_2PtCl_4-Cs_2ZrCl_6$ crystal. The dotted vertical lines show the pure electronic transition and the vertical transition.

The low-temperature spectrum, shown in Figure 1, for K_2PtCl_4, shows a progression of at least 10 lines with an average separation of *ca.* 290 cm^{-1}. The low-temperature spectrum for Cs_2PtCl_4 doped in Cs_2ZrCl_6, shown in Figure 5c, shows *two* progressions separated by about 40 cm^{-1}. The improved resolution in the mixed-crystal spectrum gives a separation of the peaks in each progression of *ca.* 283 cm^{-1}. Both are in excellent agreement with the major progression based on ν_6 of 275 cm^{-1} predicted by the simulation. The second progression in the mixed crystals has previously been assigned to a lattice mode.[36] However, the spectrum of the analogous $[PdBr_4]^{2-}$ in pure K_2PdBr_4[37] and in a mixed $Cs_2PdBr_4-Cs_2ZrBr_6$[38] system shows progressions based on both ν_6 and ν_7, as predicted in the simulation for $[PtCl_4]^{2-}$, and it seems likely that the two progressions in the mixed crystal also originate in this way.

Increasing the temperature leads to a population of the $\nu'' = 1$ levels of the inducing modes. Figures 3b and 4b show the predicted spectra originating from these levels for the ν_6 and ν_7 modes, respectively. As outlined above, this leads to progressions built upon the false origins $\Delta E^{0-0} \pm \bar{\nu}_j$. Due to the larger vibrational amplitude of the $\nu'' = 1$ levels, these have higher intrinsic intensities than those from the $\nu'' = 0$ levels, but as shown in Figures 3c and 4c, their contribution to the overall spectrum is minimal at low temperatures due to their small Boltzmann populations. As is characteristic of a vibronically induced transition,[1] increasing the temperature thus leads to an increase in intensity, and this is shown clearly in the experimental spectrum at 15 and 298 K shown in Figure 1. The progressions built upon $\Delta E^{0-0} + \bar{\nu}_j$ from the $\nu'' = 0$ and $\nu'' = 1$ levels differ only in the separation of the ν_1 levels in the excited state and are thus coincident in the harmonic model used here. The progression built upon $\Delta E^{0-0} - \bar{\nu}_j$, however, is displaced to a lower frequency by $2\bar{\nu}_j$ from these lines. As a result, the band maximum is shifted to a lower frequency as the temperature increases. The simultation, shown in Figure 5b, predicts a red shift of *ca.* 400 cm^{-1} between 4 and 300 K. This shift is also characteristic[1] of the behavior of bands whose intensity is vibronically induced. The red shift is evident in the experimental spectrum shown in Figure 1, and the shift of *ca.* 600 cm^{-1} between 15 and 298 K is comparable to that in the simulation.

(37) Rush, R. S., Jr.; LeGrand, R. G. *Inorg. Chem.* **1975**, *14*, 2543.
(38) Harrison, T. G.; Patterson, H. H.; Hsu, M. T. *Inorg. Chem.* **1976**, *15*, 3018.

Due to the lower frequency of the v_6 mode, its contribution to the overall intensity grows faster than that due to the v_7 mode as the temperature increases. The overall intensity increases, as shown in Figure 4b, by a factor of around 2 between 4 and 300 K, in excellent agreement with that observed experimentally by Martin et al.[39] and shown in Figure 1. The v_6 mode induces about 60% of the intensity at 4 K and around 67% of the intensity at 300 K.

$^1B_{1g}$ State. Excitation of an electron from the nonbonding d_{z^2} orbital into the strongly σ-antibonding $d_{x^2-y^2}$ orbital causes a lengthening of the Pt−Cl bond by *ca.* 13 pm. As predicted by Ballhausen et al.,[40] however, the square-planar structure is unstable with this arrangement and is actually a transition state between equivalent D_{2d} structures with bond angles of *ca.* 150°. The distortion corresponds to motion along the b_{2u} mode of the ground state, and this mode transforms as a_1 in D_{2d}. In these circumstances, extended progressions along the distorting mode as well as the totally symmetric breathing mode are anticipated[1] and have been observed in the analogous $^2A_{1g} \leftarrow {}^2B_{1g}$ ($d_{z^2} \rightarrow d_{x^2-y^2}$) transition in the spectrum of the square-planar $[CuCl_4]^{2-}$ ion.[41]

Analysis of the Duschinsky transformation from the ground- to the excited-state normal modes show that there is again some mixing of the e_u modes due to the change in geometry. Both of the a_1 vibrations of the excited-state have character from the v_1 (a_{1g}) and v_5 (b_{2u}) modes, which are most involved in the geometry change. FC integrals suggest that extended progressions exist in both of these totally symmetric stretching modes, with up to 20 quanta in v_5 and 10 quanta in v_1 being excited. The $^1B_{1g} \leftarrow {}^1A_{1g}$ transition is induced by the b_{2u} mode in *z* polarization and the e_u modes in *x*,*y* polarization, leading to three false origins in the low-temperature unpolarized spectrum. In addition, the presence of two equivalent D_{2d} minima results in a highly anharmonic double minima potential energy surface. The harmonic model used in the present treatment is therefore inadequate, and the progressions will actually be even more complex with intensity redistributed over the vibronic lines. The combination of these effects means that resolution of the vibrational fine structure is highly unlikely, and this transition is observed as a poorly resolved shoulder on a charge-transfer transition in the electronic spectrum[36] at *ca.* 36 500 cm^{-1}.

The SAOP functional underestimates the transition energy by around 9000 cm^{-1}, while the B3LYP functional performs worse. Inclusion of spin−orbit coupling reduces[11] the error by *ca.* 1800 cm^{-1}. The remaining error, which may, in part, be attributed to the effect of the anionic charge, is larger than that typically produced by TDDFT calculations. This band was assigned primarily because of the lack of an alternative transition in molecular orbital and ligand-field calculations.[36] This assignment warrants further investigation.

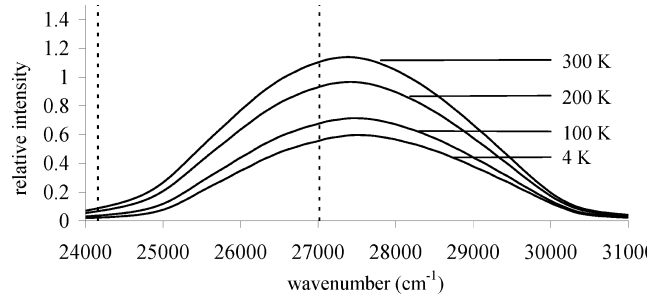

Figure 6. Low-resolution simulated spectrum for $^1B_{1g} \leftarrow {}^1A_{1g}$ as a function of the temperature. The dotted vertical lines show the pure electronic transition and the vertical transition.

As for the $^1A_{2g} \leftarrow {}^1A_{1g}$ transition, as shown in the Supporting Information, the transition moment varies approximately linearly along the possible inducing modes and is symmetric about the origin. Even at the harmonic level assumed here, progressions are not resolved in the simulated spectrum, and the effects of the highly anharmonic double minima only act to decrease this further. Figure 6 shows the predicted temperature dependence of the band. In contrast to the $^1A_{2g} \leftarrow {}^1A_{1g}$ band, the stretching e_u mode (v_7) is predicted to be a more efficient intensity generator than the bending e_u mode (v_6). However, the large value for $[(\partial M_{12})/(\partial Q_5)]_0$ and the greater vibrational amplitude for v_5 leads to the intensity of the *z*-polarized spectrum being roughly double that in the *x*,*y* polarization at low temperatures. At higher temperatures, the difference increases. Increasing the temperature again leads to transitions arising from the $v'' = 1$ levels of the inducing modes, further lowering the resolution and leading to an increase in intensity and a shift of the band maximum to a lower frequency.

^1E_g State. As this is a degenerate state, it is susceptible to a Jahn−Teller distortion. For a molecule with D_{4h} symmetry, instability occurs along b_{1g} and b_{2g} coordinates, leading to elongated and rhombic D_{2h} planar-configurations, respectively. At the BP86 level, the elongated $^1B_{3g}$ state is predicted to be *ca.* 3 kJ mol^{-1} (250 cm^{-1}) more stable than the rhombic $^1B_{1g}$ state. However, neither state corresponds to an energy minimum. The ^1E_g state arises from excitation of an electron from the degenerate $\{d_{xz,yz}\}$ orbitals into the strongly σ-antibonding $d_{x^2-y^2}$ orbital. As noted for the $^1B_{1g}$ state of the square-planar ion, occupation of this level destabilizes the planar geometry, and both $^1B_{1g}$ and $^1B_{3g}$ are unstable with respect to distortions which remove the planarity. Two equivalent C_{2v} structures are predicted with two Pt−Cl bonds elongated by *ca.* 12 pm and two Pt−Cl bonds elongated by *ca.* 16 pm, compared to the ground-state and angles of 117° and 144° between the short and long bonds, respectively. These $^1B_1$ and $^1B_2$ states differ only in whether it is d_{xz} or d_{yz} that is singly occupied.

The effect of static and dynamic Jahn−Teller vibronic coupling on the absorption spectrum of square-planar complexes has been investigated by Ballhausen[42] and Robbins,[43] within the Born−Oppenheimer approximation. In the absence of spin−orbit coupling, the Jahn−Teller effect leads

(39) (a) Martin., D. S., Jr.; Tucker, M. A.; Kassman, A. J. *Inorg. Chem.* **1966**, *5*, 1298. (b) Martin, D. S., Jr.; Tucker, M. A.; Kassman, A. J. *Inorg. Chem.* **1965**, *4*, 1682.
(40) Ballhausen, C. J.; Bjerrum, N.; Dingle, R.; Briks, K.; Hare, C. R. *Inorg. Chem.* **1965**, *4*, 514.
(41) McDonald, R. G.; Riley, M. J.; Hitchman, M. A. *Chem. Phys. Lett.* **1987**, *142*, 529.
(42) Ballhausen, C. J. *Theor. Chim. Acta.* **1965**, *3*, 368.
(43) Robbins, D. J. *Theor. Chim. Acta.* **1974**, *33*, 51.

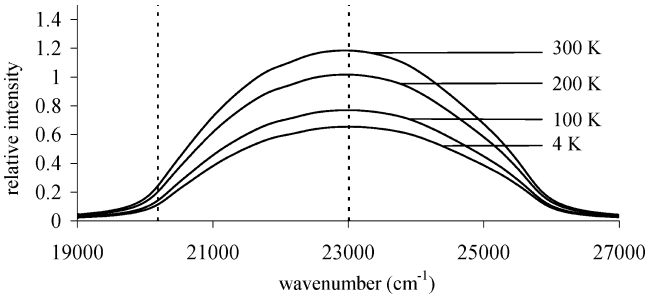

Figure 7. Low-resolution simulated spectrum for $^1E_g \leftarrow {}^1A_{1g}$ as a function of the temperature. The dotted vertical lines show the pure electronic transition and the vertical transition.

to a regular progression in the active vibration, as expected, since this vibration takes the role of a totally symmetric vibration in the distorted excited state. For small spin−orbit coupling, the progression will appear double. Strong spin−orbit coupling quenches the Jahn−Teller effect, and transitions are then seen to the two spin−orbit components of the electronically degenerate state. While the position of the $^1E_g \leftarrow {}^1A_{1g}$ transition can be unambiguously determined from the appearance of an A term in the magnetic circular dichroism (MCD) spectrum,[44] the absorption spectrum of $[PtCl_4]^{2-}$ shows only a symmetric and featureless band.[36]

At the SAOP level, the transition energy is again underestimated by *ca.* 5000 cm^{-1}. This error is roughly halved by the inclusion of spin−orbit coupling,[11] and this effect also causes considerable mixing with nearby singlet and triplet states. As noted above, the assignment of this transition is unequivocal from the MCD spectrum.

The significant change in geometry is reflected in the Duschinsky transformation from the ground- to the excited-state normal modes, which requires considerable mixing of ν_1 (a_{1g}), ν_2 (a_{2u}), ν_3 (b_{1g}), and ν_5 (b_{2u}), all of which transform as a_1 in the C_{2v} excited state. There is also some mixing of the b_1 and b_2 components of ν_6 and ν_7. FC integrals predict extended progressions in ν_1 (a_{1g}) and ν_5 (b_{2u}). In addition, the highly anharmonic double minima will lead to smearing out of the intensity in these progressions, and so a broadband with unresolved vibrational structure is predicted.

As for the other transitions studied here and as shown in the Supporting Information, the transition moment varies approximately linearly along the possible inducing modes and is symmetric about the origin. Figure 7 shows the predicted temperature dependence of this band. In *z* polarization, the bending e_u mode (ν_6) is a more efficient intensity generator than the stretching e_u mode (ν_7). However, the larger values of $[(\partial M_{12})/(\partial Q_2)]_0$ and $[(\partial M_{12})/(\partial Q_5)]_0$ and the greater vibrational amplitude for the low-frequency ν_2 and ν_5 bending modes leads to the intensity of the *x*,*y*-polarized spectrum being roughly twice that in *z* polarization at low temperatures. Experimentally, the *x*,*y*-polarized spectrum is slightly larger than the *z*-polarized spectrum, although band overlap and the presence of a tail of a charge transfer band makes quantitative estimates of relative intensity difficult. At higher temperatures, the difference increases. Increasing the temperature again leads to transitions arising from the $\nu'' = 1$ levels of the inducing modes, further lowering the resolution and leading to the increase in intensity and a shift of the band maximum to lower frequency shown in Figure 7.

5. Conclusions

The distinctive colors of transition metal complexes are commonly due to "orbitally forbidden" and, in centrosymmetric systems, Laporte-forbidden "*d*−*d*" (ligand-field) transitions. A framework for calculating the intensity distribution and vibrational fine structure in the polarized ligand-field spectrum of transition metal complexes using the Herzberg−Teller approach is introduced and used to model the spectrum of an archetypal centrosymmetric complex, the exactly square-planar $[PtCl_4]^{2-}$ ion. The model uses parameters (geometries, vibrational frequencies, and transition moments) generated using density functional calculations on the ground and excited states, allowing, for the first time, nonempirical simulation of the ligand-field trace. The model predicts the spectral polarization; the relative efficacy of the inducing modes; and the difference between the frequency of the electronic origin, the band maximum, and the vertical transition energy. It also reproduces the temperature dependence of the band intensities and the frequency of the band maxima.

In $[PtCl_4]^{2-}$, the anionic charge and, to some extent, the importance of spin−orbit coupling leads to an underestimation of the vibrational frequencies and excitation energies at the DFT and TDDFT levels. Nevertheless, the high symmetry of the complex and the relatively rich spectroscopic database available for it make it a useful system for developing the model presented in this paper. While improvements in functionals will no doubt lead to better reproduction of transition energies, the model has the potential to be a useful tool for simulating the electronic spectra of transition metal complexes, including the relative intensities of *d*−*d* and charge-transfer transitions and the roles of both vibronically and dipole-allowed transitions in centrosymmetric and noncentrosymmetric systems. The colors and electronic spectra of transition metal complexes play an important qualitative and occasionally quantitative role in probing the electronic structure in classical coordination chemistry, supramolecular chemistry, and bioinorganic chemistry.[2] This model has the potential to be a useful tool in understanding and rationalizing the relationship between the structure of a complex and its electronic spectra.

Calculations have been performed for transitions from the $^1A_{1g}$ ground state to the $^1A_{2g}$, $^1B_{1g}$, and ^1E_g excited states corresponding to spin-allowed excitation from the nonbonding d_{z^2}, the π-antibonding d_{xy}, and the π-antibonding $d_{xz,yz}$ orbitals, respectively, into the strongly σ-antibonding $d_{x^2-y^2}$ orbital. Excitation to the $^1A_{2g}$ state is accompanied by a vibrational progression in the breathing mode of the excited state, as observed experimentally. For the $^1B_{1g}$ and ^1E_g states, the excited-state geometries are distinctly nonplanar, and extended vibrational progressions in two modes are predicted. The length of these progressions and the low frequencies of

(44) McCaffery, A. J.; Schatz, P. N.; Stephens, P. J. *J. Am. Chem. Soc.* **1968**, *90*, 5730.

the vibrational modes in the excited state lead to the low resolution and broad bands observed in the experimental spectrum of this ion, which are often a feature of ligand-field spectra.

Figure 1 compares the spectral traces for the experimental and simulated spin-allowed transitions. Unfortunately, due to the underestimation of the transition energies at the TDDFT level, it has been necessary to artificially shift the calculated transition energies to resolve the bands. Nevertheless, the band shapes, relative intensities, and temperature dependence of the intensities and peak maxima are reproduced reasonably well. For the band associated with the $^1A_{2g} \leftarrow {}^1A_{1g}$ transition, these features and the vibrational fine structure are reproduced very well. For the band associated with the $^1E_g \leftarrow {}^1A_{1g}$ transition, the lack of fine structure in the experimental spectrum is reproduced, but the bandwidth is exaggerated. For this transition, spin−orbit coupling effects, including possible quenching or lessening of the Jahn−Teller distortion and an improvement in the calculated excitation energy should be included.

In contrast to earlier treatments, all possible inducing modes (stretching and bending) are included in the vibronic model described here. The intensity induced by a mode depends on both the intrinsic change in transition moment brought about by displacement along it and its amplitude. The second factor favors bending modes, since these tend to occur with lower frequency and hence higher amplitude.

Supporting Information Available: Table listing the excited-state geometries, figures showing the dependence of transition moment along the normal modes and the effect of vibronic line width on spectral resolution, and full citation for ref 27. This material is available free of charge via the Internet at http://pubs.acs.org.

IC800091Y